# Fundamental properties of spatial light modulators for the approximate optical computation of Fourier transforms: a review

**Robert W. Cohn,** MEMBER SPIE
University of Louisville
ElectroOptics Research Institute and Nanotechnology Center
Lutz Hall, Room 442, Brook and Warnock
Louisville, Kentucky 40292
E-mail: rwcohn@louisville.edu

**Abstract.** The performance of optical computers that include programmable Fourier optics depends intimately both on the physical characteristics of the particular spatial light modulator (SLM) and on the particular algorithms that map the ideal signal into the available modulation range of the SLM. Since practical affordable SLMs represent only a limited range of values in the complex plane (e.g., phase-only or quantized phase), numerous approaches have been reported to represent, approximate, encode or map complex values onto the available SLM states. The best approach depends on the space-bandwidth product (SBWP) of the signal, number of SLM pixels, computation time of encoding, the required response time of the application, and the resulting performance of the optical computer. My review of various methods, as applied to most current SLMs, which have a relatively low number of high cost pixels, leads me to recommend encoding algorithms that address the entire usable frequency plane and that emphasize the fidelity of the approximated Fourier transform over maximization of diffraction efficiency and minimization of approximation error. Frequency-dependent diffraction efficiency (due to pixel fill factor of discrete SLMs or resolution of spatially continuous SLMs) is also evaluated as a factor that can limit usable SBWP and possibly modify the choice of encoding method.
 [DOI: 10.1117/1.1409336]

Subject terms: spatial light modulators, computer generated holography, complex-valued encoding, statistical optics.

Paper OC-003 received Feb. 5, 2001; revised manuscript received July 19, 2001; accepted for publication July 20, 2001. This paper is a revision of a paper presented at the SPIE conference on Photonic Devices and Algorithms for Computing II, August 2000, San Diego, CA. The paper presented there appears (unrefereed) in SPIE Proceedings Vol. 4114.

## 1 Introduction

The ability of spatial light modulators (SLMs) to represent complex-valued images enables intensive information processing functions using the Fourier transform properties of light. Many comparisons between the speed of optical and electronic processors begin by evaluating the number of Fourier transforms operations per second that each system can perform. In these comparisons, it is common to consider the number of SLM pixels $N$ used in performing the optical Fourier transform to be identical to the number of discrete sample points in the fast Fourier transform (FFT). This assumption ignores the fact that most practical SLMs, while they may produce a range of complex values, do not produce arbitrary values of complex modulation (e.g., as shown in Fig. 1). The lack of a full range of modulation values (e.g., as exhibited by phase-only, quantized phase-only, coupled amplitude-phase, less than $2\pi$ phase modulation) can be a much more significant limitation than the finite precision arithmetic of digital processors. Thus, before beginning a comparison between digital and optical Fourier transform systems, one is faced with the problem of how to represent a desired complex value with the limited modulation range of the available SLM.

Many representation schemes have been developed since the first computer generated hologram,[2] and each method is subject to various approximation errors that reduce the total information content below that of the ideal desired signal. In some representation schemes, the space-bandwidth product (SBWP, which is equal to the number of SLM pixels $N$) is reduced. In other schemes, the fidelity of the resulting diffraction pattern (as measured by the noise and errors in the Fourier plane diffraction pattern) is degraded. Additionally, each representation scheme has a computational cost, which in some cases can exceed the computational effort of the FFT. Significantly greater computational costs can be incurred if one is attempting to produce an intensity pattern in the Fourier plane for which the phase of the design is used as a free parameter to optimize the optical performance. This problem is routinely solved by numerically intensive optimization or search algorithms for the design of fixed pattern, diffractive optical array generators. However, the solution is numerically intensive and not suited to real-time systems applications for which SLMs are intended.

This initial discussion has introduced many of the fundamental issues that one encounters in using SLMs in Fou-

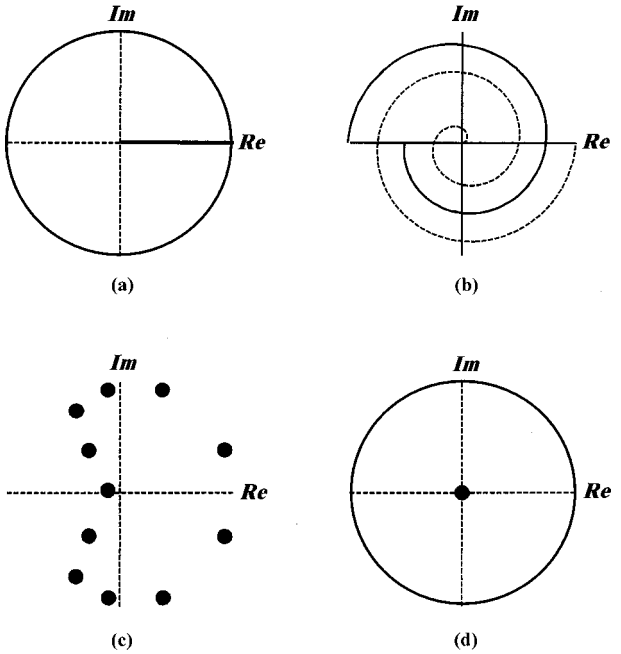


**Fig. 1** Various possible modulation ranges for SLMs: (a) phase-only and amplitude-only (thick line); (b) coupled amplitude phase, which have continuous phase ranges of $2\pi$ (solid line) and $4\pi$ (dashed line); (c) quantized; (d) biamplitude phase specifically showing amplitudes of unity and zero.[1]

rier transform applications. These issues could be overlooked by scientists new to the field of information optics, who are familiar with computer optimized designs of Fourier transform holograms, but who have not given much attention to applying diffractive design to systems that are required to adapt to unanticipated situations in real-time. For such systems, an adaptive, on-line design system is necessary and it must be structured so that it can produce an adequate design in the available response time.

This paper reviews essential properties of arrays of discretely sampled modulator pixels (i.e., *pixelated* SLMs) with particular consideration of their abilities and also limitations in terms of representing complex numbers. Various encoding schemes are considered and compared in terms of the properties of encoding range, encoding SBWP, diffraction efficiency, quality of the reconstruction, and cost of computation. These encoding methods and representative results are reviewed through Sec. 5. Section 6 considers the additional factor of limited spatial resolution of SLMs and its potential to influence the performance of the encoding methods. A frequency-dependent diffraction efficiency (which is quite similar to modulation transfer function) is defined and calculated for large fill-factor pixelated SLMs, for spatially continuous SLMs of limited spatial resolution, and for limited-resolution continuous SLMs addressed by pixelated signals. Section 6 is also a review in that the effects of limited resolution are generally well understood and easily calculated. However, Sec. 6 does present original calculations and comparisons between limited-resolution SLMs that I have been unable to locate in the archival literature. It is hoped that this review paper on the fundamental properties of SLMs will stimulate and suggest to designers of optical computing systems improved, novel

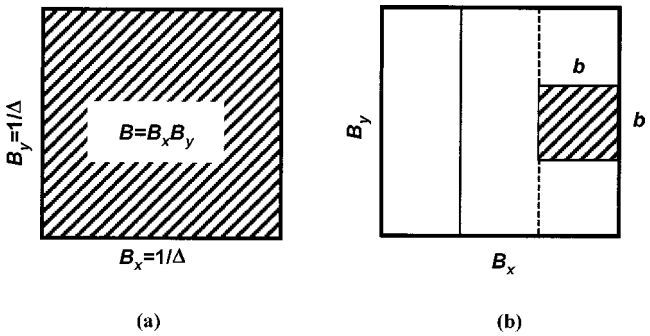


**Fig. 2** Available spatial bandwidth of SLMs and usable spatial bandwidth (shaded regions) of various encoding algorithms with the plots in the Fourier transform or reconstruction plane of the SLM: (a) available spatial bandwidth $B$ of an $n\times n$ pixel array of pitch $\Delta$ in both $x$ and $y$ and (b) usable bandwidth $B/9$ for Burckhardt's method under the constraint that the usable area is of square aspect.[1]

and more effective ways to use the inherent capabilities of SLMs.

## 2 SLM SBWP Versus Encoding SBWP

The term SBWP is used widely to describe the information capacity of a pixelated SLM in terms of its number of pixels. The number of pixels in the modulator corresponds to the number of unique, diffraction-limited resolution cells in the diffraction plane. Typically one might assume that the SLM is an $n\times n=N$ array of pixels that are equally spaced by the identical increment $\Delta$ in both $x$ and $y$. The reconstruction from this discretely sampled SLM produces periodic replicas. Each replica extends over a square area of bandwidth

$$B=B_xB_y=1/\Delta^2, \tag{1}$$

where $B_x=B_y=1/\Delta$ [see Fig. 2(a)]. I often refer to $B$ as the nonredundant bandwidth (NRB) of the modulator. The SBWP of the signal on the modulator can be distinguished from the SBWP of the modulation signal. Specifically $B_s$, the signal NRB, can be less than $B$. Figure 2(b) shows a signal spectrum in a subregion of the NRB that is $b$ units long by $b$ units wide having a bandwidth of $B_s=b^2$. This situation arises in group-oriented encoding (an example of which is presented below) because the groups (or superpixels) have a larger spacing than individual pixels, and hence, a smaller NRB. Due to the already limited resolution of SLMs and their high cost per pixel (as compared to fixed pattern computer generated holograms and diffractive optics), this loss in the effective number of pixels or SBWP could dramatically reduce the effective digital computation rate of optical Fourier transformers. In many group-oriented encoding algorithms, the superpixels are other than square. In such cases, the signal bandwidth might be nonsquare. For instance, if the pixel grouping is in the $x$ direction, then the signal NRB would be $B_s=B_xb$. However, it may be less than desirable to work with nonsquare SLMs (as well as imagers and frame grabbers.) Therefore, the nonsquare format may practically limit the useable bandwidth to $B_s=b^2$.

As an example of these concepts, consider Burckhardt's method[3] in which three adjacent pixels are used to represent one complex value. The complex amplitude of any given superpixel is effectively achieved by using the clear area of each pixel to represent amplitude, and the position of the clear area to represent phase. Fine control over phase and amplitude requires resolution much finer than the cell size, thus this method has a useable bandwidth that is much less than that set by the resolution of the modulator. If the amplitude of the modulator can be continuously varied, then a complex-valued modulation can be constructed with three pixels. Thus the usable bandwidth would be $B_x/3$ in one direction, which gives $B/9$ total usable bandwidth for an SLM that is a square array of pixels and under our assumption that the usable signal bandwidth is square [see Fig. 2(b)].

However, it can be argued that the usable bandwidth is even less. The transmittance is written as

$$a(x)=br(x)+cr(x+\Delta)+dr(x+2\Delta), \tag{2}$$

where $r(x)$ is a function (such as a rect) that describes the pixel aperture; $\Delta$ is the pitch of the pixels; and $b$, $c$, and $d$ are real positive amplitude transmittances of the pixels. The Fourier transform of this superpixel is

$$A(f_x)=R(f_x)[b+c\exp(j2\pi f_x\Delta)+d\exp(j4\pi f_x\Delta)], \tag{3}$$

where uppercase symbols indicate Fourier transformed variables. The Fourier transform of the pixel aperture function $R(f_x)$ is slowly varying with spatial frequency $f_x$ and it is ignored for this discussion (it is considered further in Sec. 6.) For $\Delta=1/(3f_0)$, Eq. (3) can be approximated as

$$A(f_0)\simeq b+c\exp(j2\pi/3)+d\exp(j4\pi/3). \tag{4}$$

Thus at the frequency $f_0=1/(3\Delta)=B_x/3$ any complex value can be produced by selecting the three weighting coefficients $b$, $c$, and $d$. The complex value in Eq. (4) is used as the design value for purposes of encoding. However, the complex value is actually frequency dependent and its value can change dramatically across the NRB $B_x/3$. The magnitude of the problem can be shown by a simple example. If $b=c=1/2$ and $d=0$, then Eq. (3) for all frequencies [with $R(f_x)=1$] is

$$A(f_x)\simeq\cos(\pi f_x/3f_0)\exp(j\pi f_x/3f_0). \tag{5}$$

Figure 3(a) is a graphical construction of the results of Eqs. (4) and (5). The designed value at $f_0$ is $A(f_0)=0.5\angle 60$ deg. This is illustrated in Fig. 3(a) as the resultant of adding the two phasors together. Also illustrated is the solid circular arc that describes the locus of the complex values over a nonredundant band of $B_x/3$. This shows that the complex values vary from $0.866\angle 30$ to $0\angle 90$ deg over the nonredundant band from $f_0/2$ to $3f_0/2$. Thus the approximation in this encoding technique is poor at the edges of the band. Depending on the accuracy required, it may be necessary to reduce the usable bandwidth further.

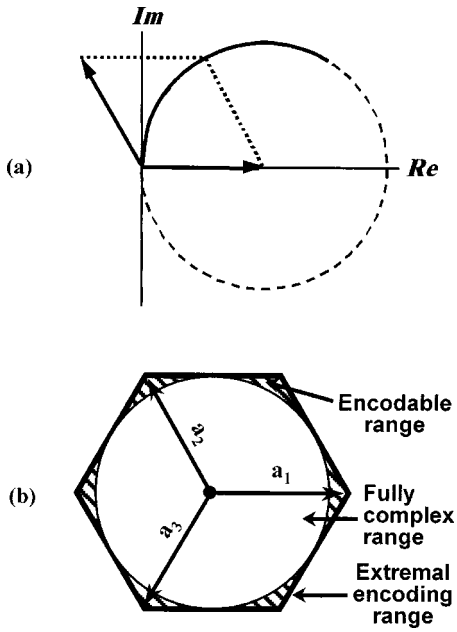


**Fig. 3** For Burckhardt's encoding method, (a) its spatial frequency dependence[1] and (b) its encoding range and fully complex encoding range.[4] In (a) the frequency-dependent complex amplitude is represented by the circular arc (solid line). The desired complex value is the intersection of the two dotted lines. The length of the arc corresponds to the values that would be found across the range of spatial frequencies $b$ in the usable band [the shaded regions in Fig. 2(b)].

## 3 Modulation Range, Encoding Range and Fully Complex Encoding Range

Modulation range is the range of values that a modulator pixel can produce. Figure 1 shows ranges for various modulators. The modulator in the example in Sec. 2 is real valued between 0 and 1 [Fig. 1(a)]. For purposes of encoding by Burckhardt's algorithm, we treat the 3 pixel superpixel as if it produces a linear combination of the three phasor values on the right side of Eq. (4).

Encoding range is the range of values that can be approximated by a particular encoding algorithm. The encoding range for Burckhardt's method is shown in Fig. 3(b). The inscribed circular region represents the fully complex encoding range. By fully complex range, we mean that the encoding method can represent any complex value out to a given radius. This maximum radius is usually limited by the passive nature of the SLM. However, some encoding algorithms [e.g., the minimum distance encoding (MDE) method introduced in Sec. 4] are not restricted in radius and can encode any value in the complex plane.

## 4 Full SBWP, Pixel-Oriented Encoding Algorithms

One of the most interesting properties of SLMs is that complex-valued encoding is possible without grouping of any kind. Thus a spectrum can be produced for which the NRB of the SLM and the encoding are identical. There are neither replications nor selected areas where there are sizeable noise patterns. This is possible by devising encodings that map each desired complex value to available values in the modulation range of the corresponding SLM pixels. Possibly the first single pixel encoding method was the ki-

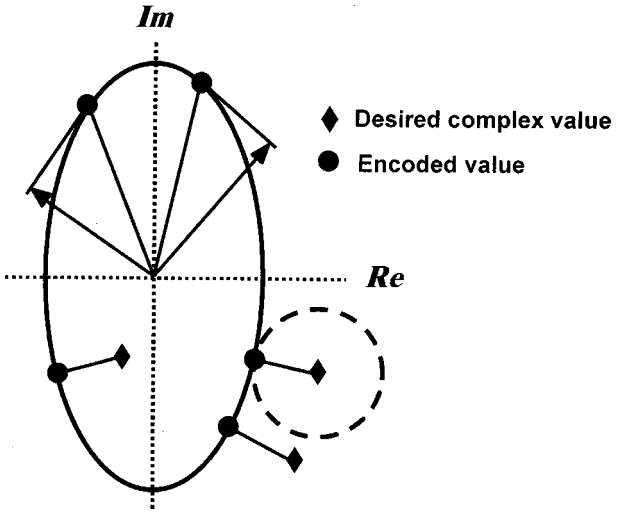


**Fig. 4** Maximum correlation peak intensity (upper half of the complex plane) and MDE methods (lower half of the complex plane) (Ref. 1).

noform, in which the magnitudes of the desired complex values are mapped on radial lines to the closest available phase-only modulation.[5] However, the original discussions of the kinoform method were not described in terms of encoding. The performance of the kinoform was improved on by iterative approaches that varied the phase degree of freedoms to improve the diffraction efficiency and accuracy of the diffraction patterns.[6] With this and continuing improvements in optimization the concepts of encoding methods lay dormant for several years. The kinoform reappeared as the phase-only matched filters for optical correlators.[7] Encoding reemerged in the work of Farn and Goodman[8] and in the work of Juday[9,10] on matched filters. Here the concept of encoding was considered from the perspective of SLMs of unusual and varied modulation characteristics. The modulators included those for which the amplitude can be written as a function of the phase, and which are referred to as amplitude-phase coupled SLMs.

### 4.1 *Encoding on the Basis of Maximum Phase Matched Energy*

The objective of the Farn and Goodman design is to maximize the intensity of the correlation peak when the training image is placed in the input of a correlator. The intensity of the correlation peak can be maximized by maximizing the magnitude of each frequency component. Thus at each frequency the phase of the filter spectrum should be conjugate to the phase of the target spectrum and the filter magnitude should be as large as possible. If the SLM could produce any value, then the filter magnitudes would be infinite. Thus the desired complex value for the corresponding SLM pixel is an infinite magnitude value with a phase that is conjugate to the phase of the target spectrum. For the modulation characteristic in Fig. 4, choosing the phase of SLM to match the desired phase (the arrows in Fig. 4) does not produce the largest magnitude in the direction of the desired phase. Instead, as shown by the construction in Fig. 4, other points on the modulator characteristic can produce even larger amplitude components along the direction of the desired phase. By focusing on other than phase-only SLMs, Farn and Goodman provided new insights into the importance of the modulator characteristic on filter design.

### 4.2 *Encoding on the Basis of Minimizing the Mean Squared Error in the Modulation Plane*

Juday generalized the Farn and Goodman method and for the first time explicitly stated the concept of mapping from the desired complex value to those values achievable[10] with the available SLM. The method begins by identifying a fully complex function that optimizes a specified cost function. Then the values are mapped to the closest value in the modulation range of the SLM, as illustrated in Fig. 4. The performance of the encoded function usually depends on a single complex value free parameter that scales the desired function. This method was originally applied to single object recognition filters, for which the method has been shown to produce optimal performance in terms of several metrics. It has since been applied to composite recognition filters and composite function Fourier transform holograms (e.g., spot array generators.) For the composite filters, the individual functions can be added together with arbitrary scale factors that provide additional degrees of freedom that can be used to minimize the mean squared mapping errors or to optimize pertinent performance metrics.[11,12] For composite functions, however, the mapping procedure is not usually optimal. This observation can be restated by saying that minimizing the mean squared error between the desired frequency plane function and the SLM values does not necessarily produce the best performance in the correlator output plane. The observation applies in a similar manner to diffractive spot array generators; that is, minimizing the mean-squared error between the desired composite function and the function produced by the modulator does not necessarily produce the best performance in the Fourier diffraction plane.

### 4.3 *Statistically Based Encoding that on Average Produces the Desired Spectrum*

The average value of a random variable can be used[13] to represent the desired complex value at each pixel of the SLM. This follows from the fact the far-field diffraction pattern is a superposition of Huygens wavefronts radiating from the SLM pixels. Therefore the wavefronts form a statistical ensemble. The law of large numbers indicates that the average pattern becomes a better approximation to the desired pattern as the number of pixels is increased.[14] This method is subject to noise effects due to the randomness of the modulation values, but the background noise (which is white over $B$) may be preferred to the background noise for minimum distance methods (which tends to be spiky). Comparisons of these methods in terms of the features of the diffraction patterns are presented in Sec. 5. Here, I review the general approach to designing pseudorandom encoding (PRE) algorithms and to evaluating the encoding range of PRE for a given SLM.

The design statement for PRE is to approximate $\mathbf{a}_c = (a_c, \Psi_c)$ the desired complex value of modulation with $\mathbf{a} = (a, \Psi)$ the modulation produced by the corresponding SLM pixel. The ordered pairs are the polar representations

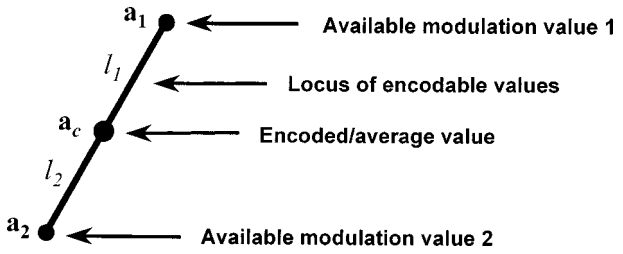


**Fig. 5** Geometry of pseudorandom biamplitude encoding. Any desired value $\mathbf{a}_c$ between the two available modulation values $\mathbf{a}_1$ and $\mathbf{a}_2$ can be encoded by pseudorandom encoding.[4]

of the complex quantities. The most general statement of the pseudorandom encoding design principal is to set $\langle \mathbf{a} \rangle = \mathbf{a}_c$, where

$$\langle \mathbf{a} \rangle = \int \mathbf{a} p(\mathbf{a}) \mathrm{d}\mathbf{a} \tag{6}$$

is the ensemble average of the complex valued random variable $\mathbf{a}$, and $p(\mathbf{a})$ is the probability density function (pdf) of the random variable. The integral equation is solved by determining a pdf that satisfies Eq. (6). The (magnitude squared) approximation error between the desired complex value and the effective average modulation has been shown to be[15]

$$\varepsilon = \langle |\mathbf{a}|^2 \rangle - |\mathbf{a}_c|^2. \tag{7}$$

This error in encoding represents the amount of energy that is diffracted into the white background speckle noise. The sum of the error components from each pixel determines the average intensity of the noise background.

For a continuous modulation range, Eq. (6) is underdetermined and there are an infinite number of pdf's that satisfy the integral equation. For a binary SLM, however, there is either a single unique solution or no solution at all. This elementary analysis provides a direct method for developing PRE algorithms and for evaluating their encoding range. Binary encoding is directly developed by substituting the pdf for the binary distribution

$$p(\mathbf{a}) = p\,\delta(\mathbf{a} - \mathbf{a}_1) + q\,\delta(\mathbf{a} - \mathbf{a}_2), \tag{8}$$

into Eq. (6), where $\delta(\cdot)$ is the Dirac delta function, $\mathbf{a}_1$ and $\mathbf{a}_2$ are a pair of complex values from the modulation characteristic and $p$ and $q = 1 - p$ are the probabilities of selecting $\mathbf{a}_1$ and $\mathbf{a}_2$. Since $p$ is a probability, its value is between one and zero. [It is clear from usage when we are referring to the binary probability $p$ and the density function $p(\mathbf{a})$.] Evaluating Eq. (6) with this pdf gives an expression for the effective complex amplitude of

$$\langle \mathbf{a} \rangle = p\mathbf{a}_1 + (1 - p)\mathbf{a}_2. \tag{9}$$

Equation (9) is recognized as the expression for a line as a function of the variable $p$. For $p = 1$, $\mathbf{a}_1$ is encoded, for $p = 0$, $\mathbf{a}_2$ is encoded and for values of $p$ between one and zero any value lying on the line segment between $\mathbf{a}_1$ and $\mathbf{a}_2$ can be encoded. This geometric interpretation (see Fig. 5) can be brought out further by considering that the desired complex value $\mathbf{a}_c$ can be expressed in terms of the two complex values $\mathbf{a}_1$ and $\mathbf{a}_2$ as

$$\mathbf{a}_c = (l_2\mathbf{a}_1 + l_1\mathbf{a}_2)/l, \tag{10}$$

where $l_1$ is the distance between $\mathbf{a}_c$ and $\mathbf{a}_1$, $l_2$ is the distance between $\mathbf{a}_c$ and $\mathbf{a}_2$, and $l = l_1 + l_2$. Clearly, the lengths can be chosen so that the desired value $\mathbf{a}_c$ can be realized by the average (or effective) value $\langle \mathbf{a} \rangle$. As Fig. 5 shows, only the range of values between $\mathbf{a}_1$ and $\mathbf{a}_2$ can be realized. Values on the same line that are outside the line segment cannot be realized by PRE because this would require that the probability $p$ either is greater than 1 or less than 0, which is not possible for a probability. Equations (9) and (10) suggest the following encoding formula for binary SLMs: For a given value of $p$, the desired complex value $\mathbf{a}_c = \langle \mathbf{a} \rangle$ is represented (i.e., encoded) by a single randomly selected value

$$\begin{aligned} &\mathbf{a} = \mathbf{a}_1 \quad \text{if} \quad 0 \leqslant s \leqslant p \\ &\mathbf{a} = \mathbf{a}_2 \quad \text{if} \quad p < s \leqslant 1, \end{aligned} \tag{11}$$

where $s$ is a uniformly distributed random number between 0 and 1. This encoding formula would be repeated for each pixel, each time with a new, independently selected random number.

The preceding analysis and geometric interpretation of binary PRE provides insight into PRE for various continuous and quantized modulation characteristics. The analysis can be used to determine the PRE encoding range for various modulation characteristics. The range is found by combining the ranges encoded by each possible pair of values from the SLM characteristic.[16] Because the binary encoding algorithm has the fewest constraints, the maximum possible range of values (a convex set) is found by this procedure. Figure 6(a) shows the convex region (shaded) that is bounded by the three possible binary encodings[4] $\mathbf{a}_1 - \mathbf{a}_2$, $\mathbf{a}_2 - \mathbf{a}_3$ and $\mathbf{a}_3 - \mathbf{a}_1$. This is the range of possible complex values that can be realized with three quantized values of modulation. Also the circular shaded region represents the range over which fully complex valued functions can be encoded. A minimum of three noncollinear modulation values are required to obtain fully complex encoding by PRE. Note that ternary encoding is similar to Burckhardt's method (Fig. 3) in that the average value encoded by ternary PRE is the vector sum

$$\mathbf{a}_c = \langle \mathbf{a} \rangle + p\mathbf{a}_1 + q\mathbf{a}_2 + r\mathbf{a}_3, \tag{12}$$

where the probabilities of selecting $\mathbf{a}_1$, $\mathbf{a}_2$ and $\mathbf{a}_3$ have total probability

$$p + q + r = 1. \tag{13}$$

In Burckhardt's method in Fig. 3, the three vectors are present simultaneously, while in ternary PRE in Fig. 6(a) the three vectors are only present in an average or virtual sense. Furthermore, the constraint of Eq. (13) leads to a different encoding range in Fig. 6(a) than for Burckhardt's method in Fig. 3(b).

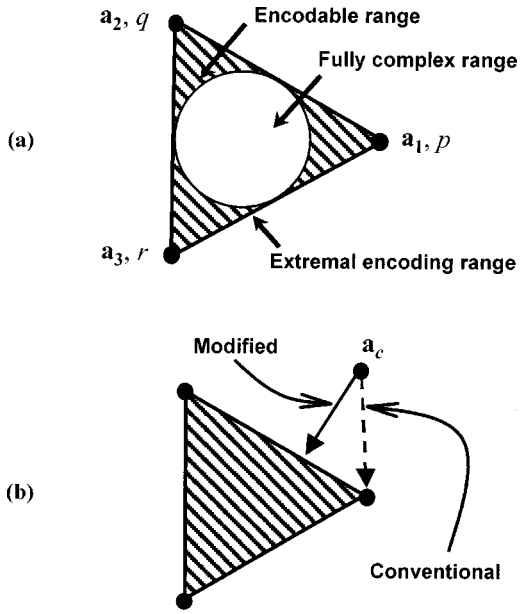


**Fig. 6** Ternary pseudorandom encoding showing (a) PRE encoding and fully complex range,[4] and (b) distinction between MD-PRE (conventional) and mMD-PRE (modified) for a ternary SLM (Ref. 17).

## 5 Blended Encoding Algorithms

The various approaches to encoding can be combined, hybridized or blended to achieve finer control and improved performance of encoding algorithms. Similar to Juday's MDE method, these new algorithms can also be fine tuned for improved performance by adjusting a few parameters. I review the blended minimum distance pseudorandom encoding[17–19] (MD-PRE) and the modified[17] MD-PRE (mMD-PRE), which are both single pixel encoding algorithms. I also present recent results on blending error diffusion (ED) with PRE (ED-PRE) (Ref. 20), which is not a full SBWP single pixel encoding algorithm. Blending PRE with MDE or ED provides a way to overcome the limited encoding range of PRE and still achieve the properties of nonspiky, white background noise. In fact, the blending of algorithms usually produces significant improvements in the fidelity of the spectrum/diffraction pattern over either encoding algorithm individually. After an introduction to the algorithms, I will present simulations that demonstrate the improvements due to blending. References 17 and 21 present experimental demonstrations of some of these encodings as well.

Figure 6(b) illustrates the difference between MD-PRE and mMD-PRE. It is specifically shown for a ternary SLM. The desired values inside the triangular region are encoded by ternary PRE. The first approach for encoding the values outside the region was to map the desired value to the closest available modulation value. This corresponds to conventional MDE. There is a second possibility that could be considered a minimum distance mapping. This would be to map the desired value to the closest value that can be encoded by PRE and then pseudorandom encode that value. This corresponds to the modified minimum distance mapping in Fig. 6(b). Figure 7 provides additional information on the various encoding methods for the ternary SLM. Figure 7(a) shows that for MDE the mapping corresponds to dividing the complex region into three decision regions. Magnitude scaling of the complex values provides no effect on this mapping. Rotating the data by a phase angle can change the performance; however, it has little effect on the test functions that are used in the simulations presented

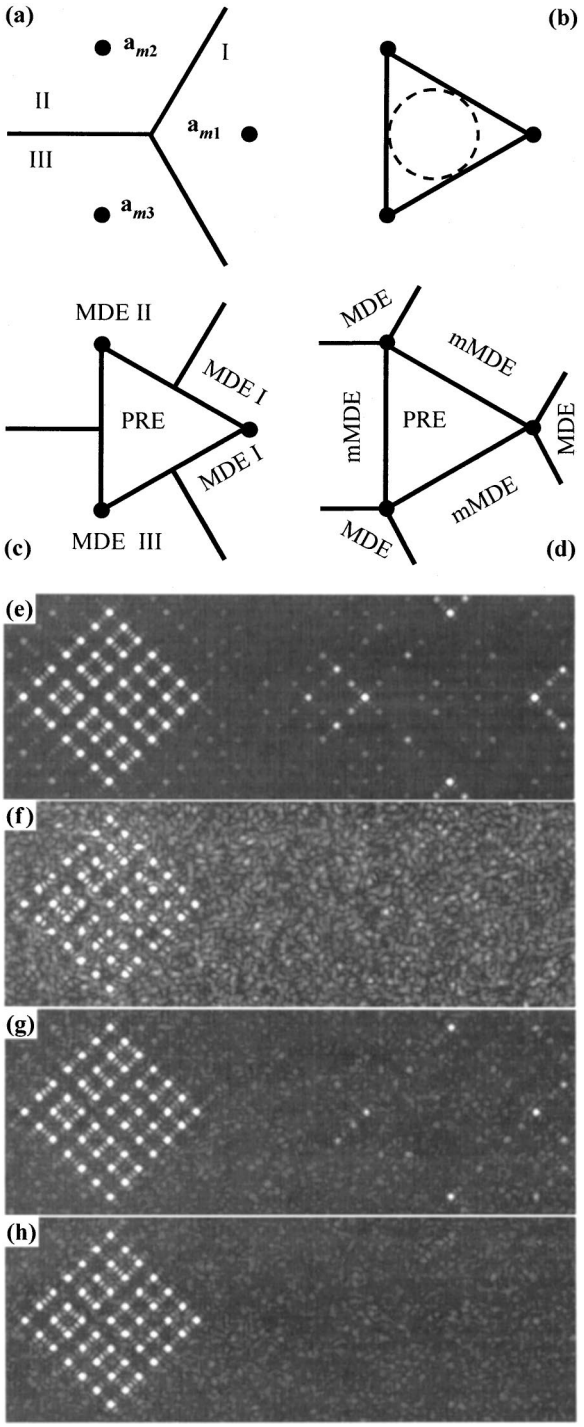


**Fig. 7** Encoding methods (a) MDE, (b) PRE, (c) MD-PRE, and (d) mMD-PRE and respective simulated far-field intensity patterns for (e) MDE with $\gamma=\infty$, (f) PRE with $\gamma=0.5$, (g) MD-PRE with $\gamma=0.80$, and (h) mMD-PRE with $\gamma=0.95$. To bring out the background noise the maximum grayscale value (full white) is 30% of the average intensity of the 49 spots. Approximately $40\times107$ resolution cells of the full $128\times128$ NRB are shown.[17]

here, since they are nearly uniformly distributed in angle. Figure 7(b) shows the PRE encoding range and the inscribed circle (radius $\gamma=0.5$) represents the fully complex encoding range. The desired complex values can be scaled to fit inside a smaller circle, but this increases the encoding error and the noise in the diffraction pattern. Figure 7(c) represents the MD-PRE algorithm. It is a combination of Figs. 7(a) and 7(b) with MDE used only when PRE is not possible. In Fig. 7(d) MDE is replaced with mMDE. The figure also indicates MDE regions. For the desired values in these regions mMDE is identical to MDE.

Figures 7(e) to 7(h) are the simulated diffraction patterns (for a desired $128\times128$ pixel modulation function) that result from using the corresponding encoding methods in Figs. 7(a) to 7(d). The intensity pattern desired is a $7\times7$ array of equal intensity spots on a negligible background of noise. For MDE [Fig. 7(e)] the pattern includes a very pronounced pattern of spikes. These are harmonics of the desired pattern and are due to the systematic mapping of the method, which is similar to hard limiting in communication systems (which produces intermodulation products at sum and difference frequencies.) PRE [Fig. 7(f)] produces a noticeable, but on average uniform, noise background. MD-PRE [Fig. 7(g)] has features of both MDE and PRE. There is both a white noise background and noise spikes, though both are weaker than either MDE or PRE individually. With mMD-PRE [Fig. 7(h)] the noise pattern is nearly identical in intensity and the noise spikes are at the level of the noise and nearly invisible to the eye. Each image shown has been optimized to produce the best combination of uniform intensity spot arrays [minimum nonuniformity (NU)] as a function of the amplitude scale factor $\gamma$. For these ''fidelity'' metrics mMD-PRE usually produces the best performance. Figure 8 demonstrates the improvement and shows how these metrics depend on the scale parameter $\gamma$. The improvements are easier to see for the four-phase than for the ternary SLM because it covers more of the complex plane, which reduces the encoding error. For the minimum value of $\gamma$ shown in the plot, each curve corresponds to PRE and for $\gamma=\infty$MD-PRE is equivalent to MDE. Both the MD-PRE and mMD-PRE have a maximum value of SPR (signal to peak noise ratio—average intensity of the 49 spots to maximum noise spike) and a minimum value of NU (nonuniformity—relative standard deviation of the 49 spots) at a specific value of $\gamma$. Achieving the best performance with intermediate values of $\gamma$ demonstrates improved performance of mMD-PRE and MD-PRE over MDE and PRE individually. In one respect, MDE is optimal. This is that it produces the highest possible diffraction efficiency.[22] However, this is at a sacrifice in fidelity. Direct design procedures[23] that require various global optimization algorithms can predistort[24] complex valued functions in ways that compensate for the nonuniformity in MDE, but this is numerically intensive.[23]

ED has proven to be an effective way to improve the appearance of halftone prints.[25] It has also been applied in slightly modified form to continuous and quantized phase-only modulators.[26] Figure 9(a) illustrates the encoding method for a continuous phase-only SLM. The value **b** at specific pixel is encoded by MDE to produce the SLM modulation **a** and the mismatch error $\boldsymbol{\varepsilon}$. This value plus values from other nearby pixels is filtered by a convolution

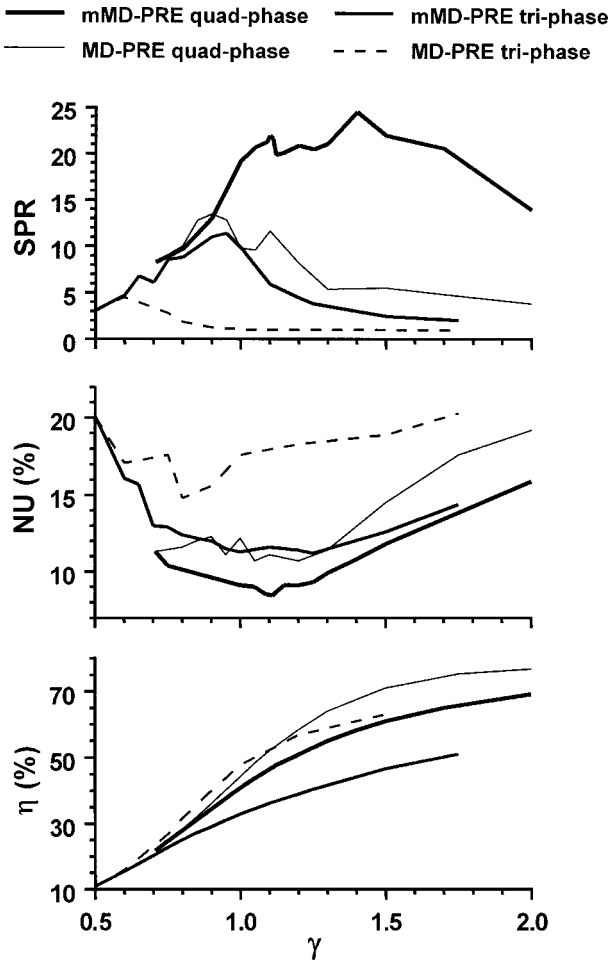


**Fig. 8** Performance of blended algorithms as a function of the scaling/blending parameter $\gamma$ for ternary phase and quad phase phase-only SLMs (Ref. 17).

kernel (say a $2\times2$ kernel) to produce $\boldsymbol{\delta}$ and then added to the desired value $\mathbf{a}_c$ to produce the next value of **b** that is again encoded by MDE. The adjacent image is the simulated diffraction pattern for ED. The filtering of the mismatch causes the noise pattern to be spatially separated from the desired pattern and the nearest neighbor encoded values to be correlated. As with the group oriented methods ED does not maximize fidelity over the NRB of the SLM. Perhaps ED can be tuned or blended to produce higher fidelity patterns. ED, because of its similarity to MDE, works even if the desired values are scaled so that $\gamma$ is greater than unity. An example of encoding when **b** exceeds unity is shown in Fig. 9(b) together with the resulting pattern when $\gamma$ is increased from 1 [in Fig. 9(a)] to 1.5. This increases SPR from less than 4 originally to 12 across the entire NRB. Figure 9(c) illustrates an MD-PRE algorithm. Inside the unit circle a biamplitude PRE method is used and MDE (i.e., the kinoform) is used for desired values outside the unit circle. The resulting diffraction pattern has an SPR of 47 and an NU of 5.8% for $\gamma=1.4$. However, the blended ED-PRE method in Fig. 9(d), has an SPR of 53 and an NU of 3.3% that is even better than MD-PRE and ED alone. The blending procedure is more complicated than previous methods in that there are now two scale parameters to be

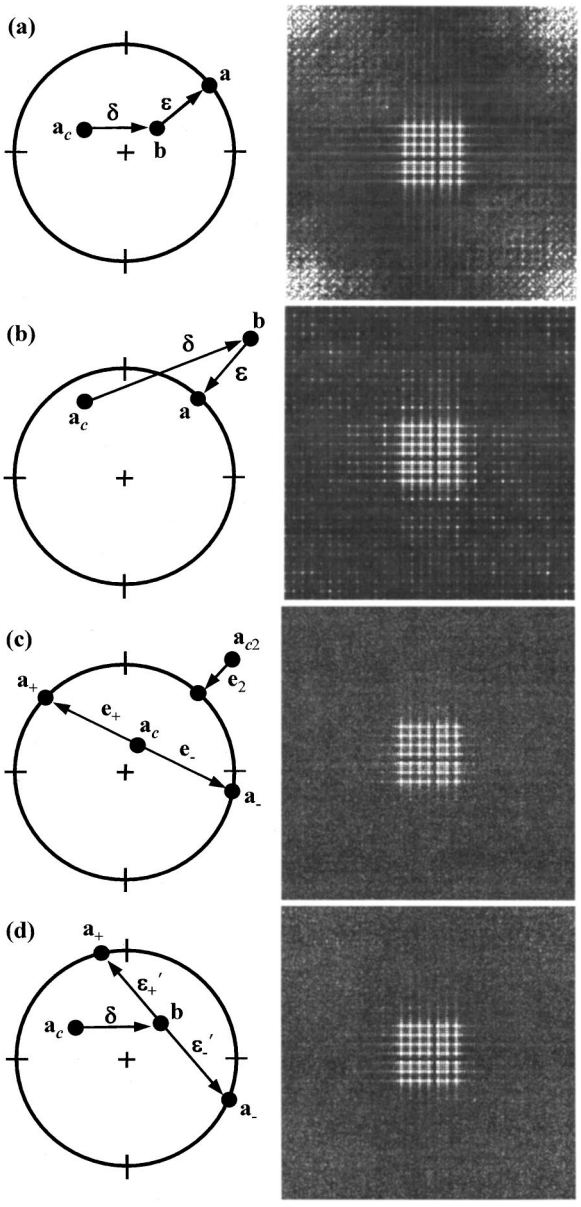


**Fig. 9** Encoding method and corresponding simulated far-field intensity patterns for (a) ED, $\gamma=1$; (b) ED, $\gamma=1.5$; (c) MD-PRE, $\gamma=1.4$; and (d) ED-PRE, $\gamma=1.3$, $\chi=0.6$. Images are saturated so that the maximum grayscale value (full white) is 3% of the average intensity of the 49 spots.[20]

varied to optimize performance. These are $\gamma$ (as before) and $\chi$, which scales the PRE encoding error. The reason for the scaling is that PRE automatically diffuses encoding error into the noise background, thus it should not also be diffused forward by ED. Values of **b** outside the unit are mapped as in Fig. 9(b). The result shown in Fig. 9(d) corresponds to using $\gamma=1.3$ and $\chi=0.6$. Careful comparison of the pattern in Fig. 9(a) to the one if Fig. 9(d) shows that the background noise pattern is weakest in the center of the image and that the ED-PRE noise pattern appears to be a diffused version of the more spiky noise pattern in Fig. 9(a).

## 6 Diffraction Efficiency Versus Usable SBWP

To this point the SLM has been modeled as an array of equally spaced point sources of pitch $\Delta$ in both $x$ and $y$. For this model, it is possible to devise encoding algorithms that produce desired diffraction patterns anywhere within the NRB. However, pixels of finite aperture (which were briefly discussed in Sec. 2) introduce a frequency-dependent rolloff $R(f_x, f_y)$ that multiplies the spectrum of the array of point sources. A consequence of the rolloff is that the intensity of the spectrum may be too low in portions of the NRB to be practically useful and thus the useful SBWP is reduced to a value less than the NRB. Making the pixel apertures as small as possible minimizes rolloff but essentially all the light is blocked by the dead space between pixels. Maximizing the pixel apertures so that there is no dead space (i.e., 100% fill factor) is 100% efficient on the optical axis ($f_x=f_y=0$) but the frequency-dependent rolloff is maximized for frequencies off the optical axis. This section further illustrates these considerations by determining the useful SBWP from maps of frequency-dependent diffraction efficiency for pixelated and spatially continuous, $2\pi$ phase-only SLMs. The effects of different fill factors and pixel aperture shapes for the pixelated SLM are compared with each other and also with spatially continuous SLMs that are subject to limited phase resolution.

Frequency-dependent diffraction efficiency is most directly appreciated by evaluating the percentage of the incident energy that can be diffracted into a single spot from the SLMs approximate implementation of a linear phase ramp. More involved analyses are possible for determining the maximum efficiency possible for *specific* diffraction pattern designs, e.g., various arrays of spots.[27,28] The simpler single-spot analysis nonetheless provides considerable insight into the efficiency-limited SBWP of various SLMs.

### 6.1 *Pixelated SLMs*

The linear phase ramp for a pixelated SLM is approximated by first modding the linear phase ramp into the $2\pi$ range of the SLM (similar to a blazed grating) and then quantizing the phase values to produce a set of stair steps. If the period of the ramp $1/f_x$ is an integer of the pixel pitch $\Delta_x$ (or more generally $m/f_x=n_x\Delta_x$, where $n_x$ and $m$ are integers), then the diffraction efficiency can be directly calculated as $\eta(f_x)=|\mathbf{a}_1(f_x)|^2$, where $\mathbf{a}_1(f_x)$ is the Fourier coefficient of the fundamental frequency $f_x$ (i.e., the position the spot is steered from the optical axis). Extending this approach to 2-D functions $g(x,y)$ that represent the SLM transmittance, the diffraction efficiency can be explicitly written as

$$\eta(f_k, f_y)=\left| f_x f_y \int_0^{1/f_x}\int_0^{1/f_y} g(x,y) \times \exp[-j2\pi(f_x x+f_y y)]\,dx\,dy \right|^2, \tag{14}$$

where $(f_x, f_y)$ is the fundamental frequency. The integral is also recognized as the Fourier transform of one period of the function, which can often be used to simplify the evaluation of Eq. (14).

For an SLM having rectangular pixels of aperture widths in $x$ and $y$ of $w=w_x=w_y$, and pitch of $\Delta=\Delta_x=\Delta_y$ (in keeping with discussions on square NRB in Sec. 2), Eq. (14) for diffraction efficiency evaluates to

$$\eta_{\mathrm{sq}}(f_x, f_y)=(w/\Delta)^4[\mathrm{sinc}(wf_x)\mathrm{sinc}(wf_y)]^2, \tag{15}$$

where $\mathrm{sinc}(x)=\sin(\pi x)/(\pi x)$. The term $p_{\mathrm{sq}}=w/\Delta$ is often referred to as the duty cycle and $A_{\mathrm{sq}}=(w/\Delta)^2$ is often referred to as the areal fill factor. For a unity duty cycle each $\mathrm{sinc}^2$ function gives efficiency that is identical to that for 1-D quantized[29] and stepped phase gratings.[30] For the case of a two phase level grating [i.e., $n_x=2$ or $f_x=1/(2\Delta)$], the efficiency is $(2/\pi)^2=0.405$, which is the identical result for a 50% duty cycle square wave. For a 2-D 100% fill factor binary grating the $\eta_{\mathrm{sq}}(\pm 1/2\Delta, \pm 1/2\Delta)=(2/\pi)^4=0.164$. For the examples developed in this section, I consider the efficiency at these corner Nyquist frequencies to be too small to be practically useful. For this particular SLM I will assume that 40.5% is the minimum required efficiency. Plotting isocontours of Eq. (15) for a 100% fill factor in Fig. 10(a) shows that the 40.5% level is nearly circular with a radius of $0.5/\Delta$. [The nearly circular contours are somewhat surprising given the rectangular separability of Eq. (15); however, plotting the contours out to higher frequencies does reveal the rectangular structure.] The useful SBWP is then $\pi/(2\Delta)^2$ or $0.79B$ where $B=1/\Delta^2$ is the NRB. The useful SBWP is still 3 to 7 times greater than for 2-pixel[31] and 3-pixel[3] group-oriented encoding algorithms (see Sec. 2). The fact that 21% of the NRB is considered to be nonuseful in this design example does motivate further research into single pixel encoding algorithms that distribute as much of the encoding error into the small nonusable areas as possible. ED and ED-MDE are a step in this direction because they do place a good deal of the light in the nonusable areas; however, much of the error, even for ED, does also appear in the usable area.

Currently the highest fill factor for pixelated SLMs is ~84% for a device in development.[32] The on-axis efficiency from Eq. (15) would be 70%. As mentioned, the rolloff is slower than for the 100% fill factor SLM, as illustrated in Fig. 10(b). The slower rolloff is reflected in that the efficiency at a radial frequency of $f_r=1/(2\Delta)$ is ~0.34 or only 84% of the efficiency of that for the 100% fill factor SLM. If one chooses to continue using the 40.5% minimum efficiency requirement then this SLM has a useful SBWP of nearly 0.6B.

It is interesting to compare the 84% fill factor, square-pixel SLM with a circular pixel SLM. For circular pixels of diameter $d$, Eq. (14) then evaluates to

$$\eta_{\mathrm{ci}}(f_r)=[\pi(d/2\Delta)^2\mathrm{jinc}(df_r)]^2, \tag{16}$$

where $\mathrm{jinc}(x)=2J_1(\pi x)/(\pi x)$, and where $J_1(x)$ is the first order Bessel function of the first kind. For $d=\Delta$, the fill factor $A_{\mathrm{sq}}=\pi(d/2\Delta)^2=0.78$ and the on-axis efficiency is 62%. Comparing the circular-pixel with the square-pixel SLM in Fig. 10(b) shows that on-axis the efficiencies are most different and that the curves are nearly identical over much of the plot away from (0, 0). If the designer can accept the lower diffraction efficiency on-axis, then the circular pixels provide the advantage of greater uniformity of diffraction efficiency across the usable SBWP. A second advantage for the SLM designer is that the increased dead space provides additional area for opaque electrodes and addressing circuitry.

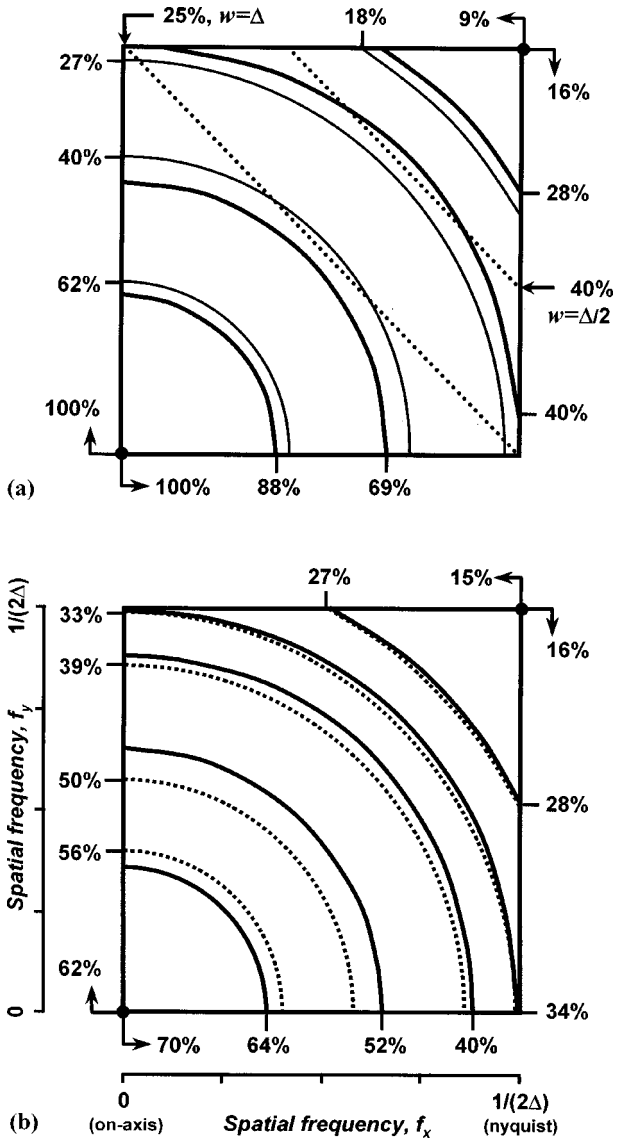


**Fig. 10** Contours of equal diffraction efficiency for phase-only SLMs: (a) SLM with square pixels of width $w=\Delta$ (thick curves), spatially continuous SLM with circularly blurred phase of blur diameter $d=\Delta$ (thin curves), and two specific curves for spatially continuous SLMs with phase blurred by squares of two different widths, and (b) SLM with square pixels of $w=0.915\Delta$ (solid curves) and SLM with circular pixel of diameter $d=\Delta$ (dotted lines). The spatial frequency coordinates and ranges in (a) are identical to those shown for (b) and correspond to one-quarter of the NRB.

### 6.2 *Spatially Continuous SLMs*

When might it be preferred to use a spatially continuous SLM over a pixelated SLM? Equation (14) can be used to help answer this question in terms of useful SBWP. Light valves are typical examples of continuous SLMs. Within the limits of scalar diffraction theory, an ideal light valve could diffract a spot to any angle with 100% efficiency.

However, phase-only light valves have limited phase resolution, which leads to frequency dependent diffraction efficiency. A useful model for this effect is to convolve the desired phase modulation with a phase point spread function[33] of the SLM. The desired modulation is a $2\pi$-modded linear phase ramp (as was used in the model of the pixelated SLM) that is then convolved with a point spread function to produce the blurred phase. The blurred phase is then evaluated using Eq. (14).

First consider the convolution of a one-dimensional phase ramp of period $1/f_x$ and a blurring function $w^{-1}\mathrm{rect}(x/w)$. The resulting blurred phase is composed of two linear phase ramps, one with the original (say positive) slope $2\pi/f_x$ over a duty cycle of $1-wf_x$ of the period and a second with a (negative) slope over the remainder of the period. Evaluation in Eq. (14) gives

$$\eta_{\mathrm{bl}}(f_x)=(1-wf_x)^2. \tag{17}$$

The efficiency is identical to the square of the duty cycle of the 1-D blaze which suggests that the negative sloped segment does not contribute to the fundamental diffraction order. This conclusion provides insight into the evaluation with 2-D blur functions. I will specifically consider square and circular blurs.

Linear phase ramps vary in only one direction, $\theta$. The 2-D blur functions, when convolved with a phase ramp, replace the desired phase values with the average phase. The average phase is identical to the value of desired phase ramp over a duty cycle of $1-w(\theta)f_r$, where $w(\theta)$ is the width of the blur function projected into the direction $\theta$. For a circular blur $w(\theta)=d$ results in a diffraction efficiency that is a circularly symmetric function of radial frequency. For a square blur function of width $w$, the efficiency can be written

$$\eta_{\mathrm{bs}}(f_x,f_y)=[1-w(f_x+f_y)]^2. \tag{18}$$

Example diffraction efficiency contours of both types of blurring are presented in Fig. 10(a). The circular curves (thin lines) are for a circular blur function of diameter $d=\Delta$. Note the 40.5% efficiency curve has a radius of $0.36/\Delta$ so with this degree of blurring the usable SBWP is $0.4B$. A single curve ($\eta=0.25$) for the square blur function of width $w=\Delta$ is also plotted. Note that the curve comes close to intersecting the circularly blurred 40% efficiency curve at $\theta=\pi/4$. The lower efficiency for the rectangularly blurred curve is reasonable when one recognizes that the rectangular blur function is longer by 1.414 in the 45 deg direction. A rectangular blur function with $w=0.51\Delta$ produces a 40.5% efficiency curve that is almost tangent to the 40.5% efficiency curve for the 100% fill factor, pixelated SLM. The useful SBWP for this degree of rectangular blurring apears to be nearly the same as that for the 100% fill factor SLM. Also note that a circular blur function with $d=0.73\Delta$ has nearly an identical 40.5% curve and useful SBWP as the 100% fill factor SLM. The reason for selecting the particular values of $w=d=\Delta$ for plotting are discussed in the next subsection.

### 6.3 *Continuous SLMs Addressed by Pixelated Signals*

Spatially continuous SLMs and light valves are often addressed by spatially discrete signals. Video monitors are composed of scan lines and frequently the video source is a frame grabber. The evaluation of the mapping from a pixelated signal to a spatially continuous, phase-blurred SLM can significantly complicate the modeling and analysis. Fortunately, there is at least one special case that can be used to gain insight into the combined effect of blurring and pixelation. The special case follows from evaluating the convolution of a blur function $\Delta^{-1}\mathrm{rect}(x/\Delta)$ with a stepped phase function of 100% duty cycle steps and period $1/f_x=n_x\Delta$. The resulting phase is identical to the phase of a blurred linear ramp with blur width $w=\Delta$. Thus with pixelation along the $x$ and $y$ directions, efficiency (at least in $x$ and $y$) can be calculated using Eq. (17) with $w=\Delta$. Therefore the Fig. 10(a) curve for the continuous SLM provides the following information on the effect of blurring with a pixelated input.

Based on the preceding discussion, the efficiency for $w=\Delta$ for the rectangular blurring and $d=\Delta$ for circular blurring is identical in $x$ and $y$ directions. The 40.5% efficiency curve for circular blur in Fig. 10(a) intersects the axes at $0.36/\Delta$. This is equivalent to saying that this degree of blurring requires that there are at least 2.7 phase steps per period, compared with 2 samples per period for the 100% fill factor pixelated SLM, to meet the minimum diffraction efficiency. In the limit of zero blur radius, the discretely addressed SLM would behave identically to the pixelated SLM.

Qualitative experience from experimental studies of phase blurring in Refs. 14, 33, and 34 leads me to believe that the effects of blurring on discretely addressed SLMs are quite a bit more severe than this idealized estimate. For real-world SLMs, I suspect that the diffraction efficiency is more severely affected both by both blurring (due to a nonabrupt, e.g., Gaussian-shaped, blur[33]) and pixelation (due to less than 100% fill factors and blurring in the write-side monitor). Despite the idealized nature of the models presented in this section, these simple results do provide useful information on the selection of SLM characteristics to achieve good utilization of optical power and SBWP.

## 7 Summary

A major goal in this review has been to identify methods that can conveniently encode the desired complex-valued modulation to the SLM. In this way it would be possible to make the most flexible use of the SLM. Certainly, many useful optoelectronic systems can be developed using precomputed, globally optimal encodings. However, precomputed solutions are not always possible or practical, especially if the processor is required to adapt to a changing environment in which there is limited prior knowledge. Thus to achieve this degree of flexibility the encoding process must not be a computational bottleneck. Also SLMs have a small number of rather costly pixels. To maximize use of the limited SBWP, methods other than the early methods of encoding from the fields of holography and computer generated holography are required for today's SLMs. The full NRB can be used by employing methods

that represent one complex value with a single SLM pixel. In using full NRB design approaches, the rolloff due to pixel fill factor and other sources of resolution loss should be considered, especially when high levels of diffraction efficiency are required over most of the NRB.

While excellent performance can be obtained by using modulation design methods that optimize performance of the SLM modulation as a function of all the pixels, these methods are time consuming and usually cannot be used on-line in an optical processor. A useful alternative is pixel-oriented encoding, which can be calculated in real time with simple operations by a serial processor. It is also possible to bring the performance of these encoding methods closer to that of the optimization methods by including a step in which some of the free parameters are adjusted to improve performance within the available computational budget of the supporting electronics. One hierarchical approach for such a design system is proposed in Ref. 21.

Fundamental properties of SLMs include their inherent SBWP, their frequency-dependent efficiency and their ability to represent complex-valued modulations with some degree of accuracy through encoding. These properties are important to consider in the design and development of numerous optical computing architectures that use SLMs in Fourier transform arrangements.[35] Future developments in the understanding of SLM properties and encoding could further improve the optical performance and reduce the computational complexity needed to demonstrate real-time Fourier transform processors that are based on limited modulation range SLMs.

## Acknowledgments

This paper reports on and reviews findings that were supported by the National Aeronautics and Space Administration (NASA) cooperative agreement No. NCC5-222, Office of Naval Research (ONR) Grant No. N00014-96-1-1296, and the Ballistic Missile Defense Organization (BMDO) through the Air Force Research Laboratory Grant F19628-99-C-0084. Figures cited from Ref. 1 are adapted from that work and reprinted with the permission of Cambridge University Press. Also the figures cited from Optical Society of America publications are adapted from the original publications with the permission of Optical Society of America.

## References

1. R. W. Cohn and L. G. Hassebrook, ''Representations of fully complex functions on real-time spatial light modulators,'' Ch. 15, pp. 396–432 in *Optical Information Processing*, F. T. S. Yu and S. Jutamulia, Eds. (Cambridge University Press, Cambridge, 1998).
2. B. R. Brown and A. W. Lohmann, ''Computer-generated binary holograms,'' *IBM J. Res. Dev.* 160–168 (1969).
3. C. B. Burckhardt, ''A simplification of Lee's method of generating holograms by computer,'' *Appl. Opt.* **9**, 1949 (1970).
4. R. W. Cohn and M. Duelli, ''Ternary pseudorandom encoding of Fourier transform holograms,'' *J. Opt. Soc. Am. A* **16**, 71–84 () and ''errata,'' 1089–1090 (1999).
5. L. B. Lesem, P. M. Hirsch and J. A. Jordon, Jr., ''The kinoform: A new wavefront reconstruction device,'' *IBM J. Res. Dev.* **13**, 150–155 (1969).
6. N. C. Gallagher and B. Liu, ''Method for computing kinoforms that reduces image reconstruction error,'' *Appl. Opt.* **12**, 2328–2335 (1973).
7. J. L. Horner and P. D. Gianino, ''Phase-only matched filtering,'' *Appl. Opt.* **23**, 812–816 (1984).
8. M. W. Farn and J. W. Goodman, ''Optimal maximum correlation filter for arbitrarily constrained devices,'' *Appl. Opt.* **28**, 3362–3366 (1989).
9. R. D. Juday, ''Correlation with a spatial light modulator having phase and amplitude cross coupling,'' *Appl. Opt.* **28**, 4865–4869 (1989).
10. R. D. Juday, ''Optimal realizable filters and the minimum Euclidean distance principle,'' *Appl. Opt.* **32**, 5100–5111 (1993).
11. B. V. K. Vijaya Kumar and D. W. Carlson, ''Optimal trade-off synthetic discriminant function filters for arbitrary devices,'' *Opt. Lett.* **19**, 1556–1558 (1994).
12. M. Montes-Usategui, J. Campos, and I. Juvells, ''Computation of arbitrarily constrained synthetic discriminant functions,'' *Appl. Opt.* **34**, 3904–3914 (1995).
13. R. W. Cohn and M. Liang, ''Approximating fully complex spatial modulation with pseudo-random phase-only modulation,'' *Appl. Opt.* **33**, 4406–4415 (1994).
14. R. W. Cohn and M. Liang, ''Pseudorandom phase-only encoding of real-time spatial light modulators,'' *Appl. Opt.* **35**, 2488–2498 (1996).
15. R. W. Cohn, ''Pseudorandom encoding of fully complex functions onto amplitude coupled phase modulators,'' *J. Opt. Soc. Am. A* **15**, 868–883 (1998).
16. R. W. Cohn, ''Analyzing the encoding range of amplitude-phase coupled spatial light modulators,'' *Opt. Eng.* **38**, 361–367 (1999).
17. M. Duelli, M. Reece, and R. W. Cohn, ''Modified minimum-distance criterion for blended random and nonrandom encoding,'' *J. Opt. Soc. Am. A* **16**, 2425–2438 (1999).
18. L. G. Hassebrook, M. E. Lhamon, R. C. Daley, R. W. Cohn, and M. Liang, ''Random phase encoding of composite fully-complex filters,'' *Opt. Lett.* **21**, 272–274 (1996).
19. R. W. Cohn and W. Liu, ''Pseudorandom encoding of fully complex modulation to bi-amplitude phase modulators,'' in *Proc. Optical Society of America Topical Meeting on Diffractive Optics and Micro Optics*, 1996 OSA Technical Digest Series, Vol. 5, 237–240, Boston (1996).
20. L. Ge, M. Duelli, and R. W. Cohn, ''Improved fidelity error diffusion by blending with pseudorandom encoding,'' *J. Opt. Soc. Am. A* **17**, 1606–1616 (2000).
21. L. Ge, M. Duelli, and R. W. Cohn, ''Enumeration of illumination and scanning modes from real-time spatial light modulators,'' *Opt. Express* **7**, 403–416 (2000).
22. F. Wyrowski, ''Upper bound of the diffraction efficiency of diffractive phase elements,'' *Opt. Lett.* **16**, 1915–1917 (1991).
23. J. N. Mait, ''Understanding diffractive optic design in the scalar domain,'' *J. Opt. Soc. Am. A* **12**, 2145–2158 (1995).
24. D. Jared and D. Ennis, ''Inclusion of filter modulation in synthetic discriminant function construction,'' *Appl. Opt.* **28**, 232–239 (1989).
25. R. W. Floyd and L. Steinberg, ''An adaptive algorithm for spatial grayscale,'' Proc. SID **17**, 78–84 (1976).
26. S. Weissbach, F. Wyrowski, and O. Bryngdahl, ''Digital phase holograms: coding and quantization with and error diffusion concept,'' *Opt. Commun.* **72**, 37–41 (1989).
27. V. Arrizon and M. Testorf, ''Efficiency limit of spatially quantized Fourier array illuminators,'' *Opt. Lett.* **22**, 197–199 (1997).
28. V. Arrizon, E. Carreon, and M. Testorf, ''Implementations of Fourier array illuminators using pixelated SLM: efficiency limitations,'' *Opt. Commun.* **160**, 207–213 (1997).
29. W. J. Dallas, ''Phase quantization—a compact derivation,'' *Appl. Opt.* **10**, 673–674 (1971).
30. H. Dammann, ''Spectral characteristics of of stepped phase gratings,'' *Optik (Stuttgart)* **53**, 409–417 (1979).
31. J. M. Florence and R. D. Juday, ''Full complex spatial filtering with a phase-mostly DMD,'' in *Wave Propagation and Scattering in Varied Media II*, V. K. Varadan, Ed., *Proc. SPIE* **1558**, 487–498 (1991).
32. Private communication with K. Bauchert, Boulder Nonlinear Systems, Inc..
33. M. Duelli, L. Ge, and R. W. Cohn, ''Nonlinear effects of phase blurring on Fourier transform holograms,'' *J. Opt. Soc. Am. A* **17**, 1594–1605 (2000).
34. R. W. Cohn, A. A. Vasiliev, W. Liu, and D. L. Hill, ''Fully complex diffractive optics by means of patterned diffuser arrays: Encoding concept and implications for fabrication,'' *J. Opt. Soc. Am. A* **14**, 1110–1123 (1997).
35. A. D. McAulay, *Optical Computer Architectures*, Cambridge, Wiley, New York (1991).

**Robert W. Cohn** is a professor of electrical and computer engineering and directs the ElectroOptics Research Institute and Nanotechnology Center at the University of Louisville. He received his PhD from Southern Methodist University and his MS and BS degrees from the University of Kansas, Lawrence, all in electrical engineering. Prior to joining the University of Louisville, from 1978 to 1989, Cohn was a member of the technical staff, with Texas Instruments in Dallas. There he performed research on deformable

mirror spatial light modulators for optical information processing, surface acoustic wave devices and microwave hybrid circuits for electronic signal processing, and tracking algorithms for imaging IR missile seekers. Currently he continues research on the application and characterization of spatial light modulators, as well as related studies on the fabrication of nanostructures for guiding, scattering and diffraction of light. Cohn is a fellow of the Optical Society of America.